Luminescence properties of the x-ray storage phosphor $BaBr_2:Ce^{3+}$

2004 J. Phys.: Condens. Matter 16 1489

(http://iopscience.iop.org/0953-8984/16/8/028)

INSTITUTE OF PHYSICS PUBLISHING JOURNAL OF PHYSICS: CONDENSED MATTER

J. Phys.: Condens. Matter **16** (2004) 1489–1500 PII: S0953-8984(04)70632-3

Luminescence properties of the x-ray storage phosphor $BaBr_2:Ce^{3+}$

G Corradi[1,2], M Secu[1], S Schweizer[1,3] and J-M Spaeth[1]

[1] Department of Physics, University of Paderborn, Warburger Strasse 100, D-33098 Paderborn, Germany
[2] Research Institute for Solid State Physics and Optics, Hungarian Academy of Sciences, Budapest, PO Box 49, H-1525, Hungary

E-mail: schweizer@physik.upb.de

Received 14 October 2003
Published 13 February 2004
Online at stacks.iop.org/JPhysCM/16/1489 (DOI: 10.1088/0953-8984/16/8/028)

Abstract

Photoluminescence studies on single-crystal samples of the x-ray storage phosphor orthorhombic $BaBr_2:Ce^{3+}$ show the existence of three luminescent Ce sites with distinct emission and excitation spectra. The isolated Ce^{3+} emits only at low temperatures, while the two other Ce^{3+} sites are charge compensated and active also at room temperature. One of the charge compensators was identified as a monovalent cation impurity, which was confirmed by the investigation of $BaBr_2:Ce^{3+}$ co-doped with potassium. The same charge-compensated sites serve as efficient emission sources during the read-out of stored images following x-ray exposure. Read-out is a photostimulated luminescence (PSL) process initiated by the excitation of x-ray-induced F-type trapped electron centres in the visible region. There are two different PSL processes, corresponding to the two kinds of charge-compensated Ce centre, each involving trapped electron and trapped hole centres of a slightly different kind in the vicinity of the charge-compensated Ce sites.

1. Introduction

Information is stored in x-ray storage phosphor screens in the form of electron and hole trap centres stable at room temperature. Upon photostimulation of one type of centre, usually the electron trap centres, the liberated electrons recombine with the hole trap centres, resulting in luminescence at nearby activators which are usually rare-earth dopant ions. For a recent review see [1]. Promising candidates for storage phosphors with high spatial resolution are rare-earth-activated fluorobromozirconate (ZBLAN) glass ceramics containing PSL-active $BaBr_2$ nano-particles [2–5]. Due to reduced light scattering these glass ceramics may have better

[3] Author to whom any correspondence should be addressed.

spatial resolution than the currently used BaFBr:Eu powdered crystal phosphors. For a better understanding of the PSL mechanism in these glass ceramics it is essential to investigate the x-ray storage and read-out processes of bulk $BaBr_2$ phosphors for comparison. The glass base of the glass ceramic itself shows no PSL.

The stable phase of barium bromide at room temperature has the orthorhombic $PbCl_2$ structure (space group D_{2h}^{16}, $Pnma$, $Z = 4$) with the lattice parameters $a = 0.8276$ nm, $b = 0.4956$ nm, and $c = 0.9919$ nm [6]. The Ba^{2+} sites, where the incorporation of rare earths is expected, occupy crystallographically equivalent positions having nine neighbouring Br anions at distances between 0.321 and 0.383 nm in a tricapped trigonal prism configuration (see e.g. figure 1 in [3]). Though the elementary cell has a centre of inversion, the local symmetry of all cation and anion sites corresponds only to the point group C_S with a single symmetry plane parallel to the ac-plane. There are two different Br sites with fourfold and fivefold cation coordination, respectively. In undoped crystals stable F centres (electrons trapped in Br^- vacancies) have been produced by electrolytic or additive coloration and attributed to Br^- sites with fourfold Ba^{2+} coordination [7, 8]. However, both types of Br^- vacancy can trap electrons, at least temporarily: the decay of the respective F centres has recently been observed at liquid helium temperatures by detecting the EPR spectrum via the afterglow in $BaBr_2$:Eu^{2+} crystals following x-ray irradiation [9]. Using conventionally detected EPR and optical absorption on crystals x-irradiated and measured at 77 K, stable F-type centres could only be observed if additional potassium doping was applied [10]. The latter may be F centres perturbed by adjacent K^+ ions as suggested by their slightly redshifted absorption bands [10]. Along with F centres x-irradiation also produces V_K-type trapped hole centres where the hole is essentially localized as a relaxed Br_2^- molecule ion, but with appreciable overlap of the hole with a third Br^- ion [11]. The majority of F- and V_K centres recombines near 106 K, showing thermoluminescence in the 430–490 nm region [9]. A similar emission is also present in the x-ray luminescence and the afterglow following low temperature x-irradiation [9]. One hour after switching off the x-ray, the intensity of this recombination luminescence is comparable to that of excitonic (in undoped) or activator-related (in Eu-doped $BaBr_2$) emission bands whereby the latter emissions decay faster [12]. The excitonic processes of anionic Frenkel pair formation, very efficient in the alkali halides with NaCl structure [13], seem to lead to no stable radiation centres in orthorhombic $BaBr_2$.

After x-irradiation at room temperature, Eu-doped $BaBr_2$ shows an important PSL effect which can be used to recover the stored x-ray image [3, 9, 14, 15]. In this paper we are concerned with the luminescence, excitation, and stimulation processes in Ce-doped material. As we will see, the efficiency of the PSL effect in $BaBr_2$:Ce^{3+} is fairly comparable to that of commercially used BaFBr:Eu^{2+}.

The characteristic double-band emission of the Ce^{3+} ion occurs from the lowest crystal field component of the $5d^1$ excited state to the two levels of the ground state; the well shielded $4f^1$ ground state is split by spin–orbit coupling into two levels, $^2F_{7/2}$ and $^2F_{5/2}$, separated by about 2000 cm^{-1} (for a review see [16–18]).

2. Experiment

2.1. Sample preparation

Single crystals of orthorhombic $BaBr_2$ were grown in the Paderborn crystal growth laboratory using the Bridgman method with a quartz glass ampoule, $SiBr_4$ atmosphere and $BaBr_2$ powder to which 1000 M ppm of $CeBr_3$ were added. Crystals co-doped with 1000 M ppm of KBr were also prepared, as well as undoped samples. The usual technique was modified for

careful annealing and slow cooling through the cubic–orthorhombic phase transformation near 800 °C [19]. Prior to crystal growth the $BaBr_2$ powder was dried in vacuum with subsequent melting in a $SiBr_4$ atmosphere to reduce oxygen contamination. The concentration of monovalent alkali impurities originating from the raw materials has been estimated to be of the order of several ppm.

2.2. Experimental set-up

The photoluminescence (PL) and photostimulated luminescence (PSL) spectra were recorded with a single-beam spectrometer containing two 0.25 m double monochromators (Spex), one for excitation and one for emission. The samples were excited either with a halogen lamp in the visible spectral range or with a deuterium lamp in the ultraviolet range. The emission and excitation spectra were detected using a photomultiplier and single-photon counting. The emission and excitation spectra are not corrected for instrumental response. The emission sensitivity is mainly due to the sensitivity of the photomultiplier and is relatively flat in the spectral range from around 390 up to 850 nm. Even in the region of decreasing sensitivity below 390 nm the estimates show that the absolute emission peak positions given are reliable within a few nanometres, depending on the linewidth. Similar estimates, based on the spectral properties of the lamps and the spectral response of the monochromator, are valid for the excitation peaks and the components of the stimulation spectra. Therefore, the corrections would not qualitatively change any of the statements. For low temperature measurements a continuous flow helium cryostat was used. Prior to PSL measurements the samples were irradiated at room temperature (RT) using a tungsten anode at 50 kV and 30 mA for 5 min.

3. Experimental results

3.1. Spectra of $BaBr_2$:Ce^{3+}

Photoluminescence measurements performed at 300 K in $BaBr_2$:Ce^{3+} show a resolved luminescence doublet peaking at 345 and 372 nm, and a second band with an unresolved peak at 420 nm (figure 1). These can be assigned to two Ce^{3+} luminescent sites, denoted by A and B, respectively. A shoulder is observed at about 475 nm, which is apparently unrelated to Ce, since an emission in this spectral region can be observed in all our Ce-free crystals as well. Excitation spectra consisting of several partly resolved components are shown in the same figure. For site A the excitation spectrum is shown for the emission wavelength 345 nm (dashed curve); the one for 372 nm is essentially identical. The dotted excitation spectrum is mainly due to site B.

After cooling to 20 K the emission spectra are better resolved, slightly blueshifted and show additional features (see figure 2). Site A luminescence is observed at 342 and 370 nm, and site B luminescence now has a resolved doublet at 382 and 410 nm as shown by solid curves in parts (a) and (b) of figure 2, respectively. The latter spectrum also contains some admixture from both peaks of the site A luminescence, manifested in the small peak at 342 nm and the broadening of the 382 nm peak. In addition to A and B, a third doublet is observed at 330 and 353 nm, assigned to a further site denoted as the C site (figure 2, solid curve in part (c)). The splitting of all doublets is at about 2000 cm^{-1} which is consistent with the assignment to cerium luminescences. The unspecific emission is also better resolved at about 460 nm and has no partner 2000 cm^{-1} away (no shoulder near 421 nm can be discerned either). Time-resolved PL measurements for the 460 nm band have shown that at least two components are involved. The decay times are in the range of tens of microseconds which is rather long compared to the

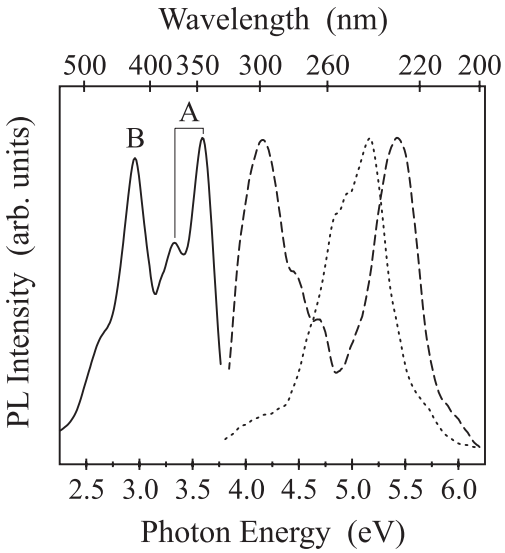

Figure 1. Normalized excitation and photoluminescence spectra of $BaBr_2$:Ce^{3+}. The photoluminescence (solid curve) was excited at 245 nm; the excitation spectra were detected at 345 nm (dashed curve) and 420 nm (dotted curve), respectively. The spectra were recorded at room temperature.

Table 1. Wavelengths (nm) of the observed bands for the A, B, and C sites of luminescent Ce^{3+} centres (bold numbers indicate the most intense line of the respective group; cross-effects described in the text are marked by superscripts).

Site	Temp. (K)	PL excitation	PL emission	PSL emission	PSL stimulation
A	RT	230, 264[c], 275[c], **298**, 308	**345**, 372	**347**, 375	∼480
	20	225, 254, **293**, ∼310	**342**, 370	—	—
B	RT	$220^{(ox)}$, ∼$\mathbf{240}^{(ox)}$, ∼$255^{(ox)}$, ∼303	**420**	**420**	∼550
	20	$207^{(ox)}$, ∼$222^{(ox)}$, $\mathbf{235}^{(ox)}$, $254^{(ox)}$, 305	382, **410**	385, **417**	507, **555**, ∼600, 725
C	RT	—	—	—	—
	20	244, 261, **278**, 302	330, **353**	—	—

lifetimes of all Ce^{3+} emission bands (below the temporal limit of our equipment). This again supports the view that the 460 nm shoulder is of different origin. Ce^{3+} emissions usually have lifetimes of the order of some tens of nanoseconds (see e.g. [17]).

Excitation spectra for each Ce^{3+} doublet are shown by dashed curves in figure 2; the observed band positions are summarized in table 1. The 330 nm peak of site C is a clearly separated luminescence peak, practically unaffected by overlap with other emission lines; accordingly, the corresponding excitation spectrum (dashed curve in figure 2, part (c)) is expected to be free from admixtures from other sites. All lines in this spectrum have similar linewidths, smaller than most lines seen in the other excitation spectra, which is another reason for their assignment to the same site.

The excitation spectrum taken at 342 nm (dashed curve in figure 2, part (a)) contains, in addition to the peaks at 225, 254, and 293 and a shoulder near 310 nm assigned to site A,

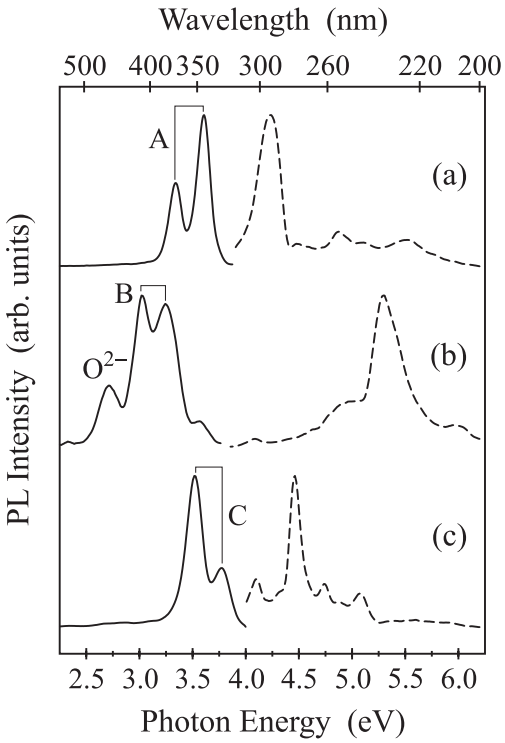

Figure 2. Normalized excitation (dashed curves) and photoluminescence spectra (solid curves) of $BaBr_2:Ce^{3+}$. (a) PL, excited at 295 nm, and PL excitation, detected at 342 nm; (b) PL, excited at 235 nm, and PL excitation, detected at 410 nm; (c) PL, excited at 275 nm, and PL excitation, detected at 330 nm. All spectra were recorded at 20 K.

also very small features near 244 and 278 nm attributable to site C (see part (c) in figure 2). More pronounced admixture of C-type features is observed at higher temperatures between 150 K and room temperature, i.e. in the whole measured range where the C-type luminescence is 'silent' (see figure 1, dashed curve; in particular the shoulders near 261 and 278 nm can be clearly seen). This indicates a quenching mechanism via site A. In fact, for a C-type excitation at 278 nm, the transition from C- to essentially A-type emission can be observed in the temperature range from 110 to 150 K.

The B-type excitation spectrum seems to extend further to the UV region than the other types (dashed curve in figure 2, part (b), shown for the 410 nm luminescence which is relatively well separated from other Ce^{3+} emission bands). As absorption in single-crystal $BaBr_2$ films starts only above 6 eV [20], host excitation can be excluded. However, most features of type B may have interference from centres possibly related to oxygen. First, the broad Ce-independent luminescence at 460 nm has excitation bands at 220 and 240 nm. Second, PL measurements made in oxygen-doped $BaBr_2$ also show luminescence with long radiative lifetimes in the range of tens of microseconds peaking at 425 and 490 nm, both having similar excitation peaks at 210, 240–260, and ∼290 nm, where the one near 240 nm has maximal intensity (see [21]). So in $BaBr_2:Ce^{3+}$ part of the observed large 235 nm peak and its shoulders at ∼222 and 254 nm, and most or even all of the 207 nm excitation peak, may come from some oxygen background. The B-type centres may also serve as activator centres collecting the excitation energies of some nearby centres e.g. due to oxygen contamination; this might explain the large intensity

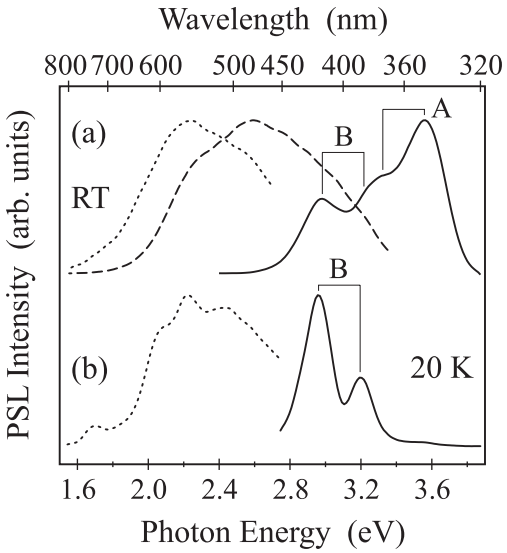

Figure 3. Normalized PSL and PSL stimulation spectra of $BaBr_2:Ce^{3+}$ after x-irradiation at room temperature. The PSL was stimulated at 580 nm (part (a), solid curve) and 550 nm (part (b), solid curve), respectively; the stimulation was detected at 345 nm (part (a), dashed curve) and 420 nm (parts (a) and (b), dotted curves), respectively. The spectra were recorded at room temperature (part (a)) and at 20 K (part (b)), respectively.

of the excitation band near 235 nm. The 305 nm excitation peak in contrast is assumed to belong nearly exclusively to Ce at the B site (though similar to the 302 nm peak seen in the C-type excitation spectrum), otherwise an unrealistically large Stokes shift for B would result.

The photostimulated luminescence (PSL) spectrum measured at RT after x-irradiation (figure 3, part (a)) is similar to the PL shown in figure 1, but has no 'Ce-independent shoulder' at 475 nm, once more indicating the different origin of this shoulder seen in PL. The PSL band at 347 nm with the shoulder at 375 nm corresponds to the A site, while the band at 420 nm to the B site. The PSL results are summarized and compared with PL data in table 1. The PSL stimulation spectra, also shown in figure 3, part (a), are broad, weakly structured bands of similar width near 480 and 550 nm for the emission maxima 347 and 420 nm, respectively. Decreasing the measurement temperature to 20 K (with the x-irradiation still at RT) the PSL reduces to a single doublet peaking at 386 and 417 nm, which very nearly corresponds to the PL assigned to the B site (see figure 3, part (b)). The corresponding PSL stimulation spectrum, included in the same figure, has partly resolved features at 507, 555, 600, and 725 nm. These features of the low temperature stimulation spectrum show a clear resemblance to the peaks denoted in [8, 15] by D, C, B, and A peaking at 522, 575, 601, and 725–730 nm, respectively, of the F-centre absorption spectrum of undoped $BaBr_2$.

The efficiency of the PSL at room temperature is crucial for its application as a storage phosphor [1]. We carried out preliminary read-out experiments for $BaBr_2:Ce^{3+}$ and $BaFBr:Eu^{2+}$ single crystals by measuring the decay of each PSL type separately and integrating over the full decay, using in each case the same monochromators, the same stimulation at 580 nm (which is optimal in all cases but the A-type emission in $BaBr_2:Ce^{3+}$), and the respective optimal observation wavelengths. In $BaBr_2:Ce^{3+}$, the integrated intensity found for the A-type emission at 350 nm is about twice as large as that measured for the B-type emission at 420 nm, in accordance with figure 3, part (a). (Note that there is some reabsorption of B-type

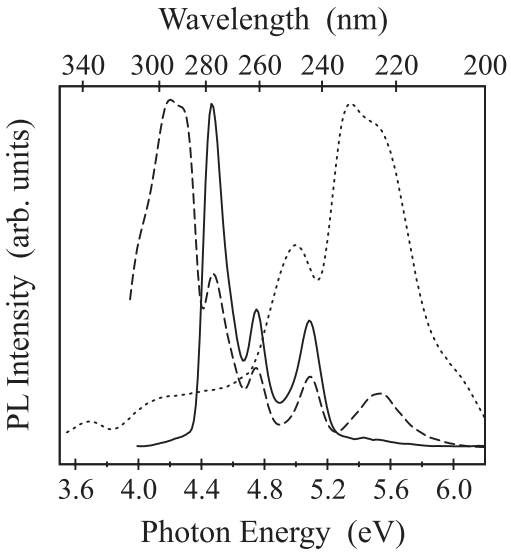

Figure 4. Normalized excitation spectra of $BaBr_2:K:Ce^{3+}$, detected at 330 nm (C type, solid curve), 342 nm (A type, dashed curve), and 410 nm (B type, dotted curve), respectively. The spectra were recorded at 20 K.

emission favouring A-type luminescence.) The sum of these two integrals is equal to a few tenths of a similar integral measured for the single PSL type of $BaFBr:Eu^{2+}$ at 395 nm. This ratio is underestimated due to the decreased sensitivity of the set-up near 350 nm and the non-optimal stimulation of the A-type luminescence; its precision is also limited by the hygroscopic character of the $BaBr_2$ samples. Taking into account all circumstances our estimates indicate that, choosing appropriate broadband read-out strategies for $BaBr_2:Ce^{3+}$, total PSL efficiencies nearly comparable to that of $BaFBr:Eu^{2+}$ can be achieved.

3.2. Spectra of $BaBr_2:K:Ce^{3+}$

Photoluminescence measurements recorded at room temperature in $BaBr_2:K:Ce^{3+}$ show only luminescence doublet A, while at low temperatures all three doublets A, B, and C can still be observed. Compared to $BaBr_2:Ce^{3+}$, there are some other modifications as well (see figure 4). The excitation spectrum of the C-type 330 nm emission (solid curve) now exhibits only three maxima, at 244, 261, and 278 nm. These peaks again reappear in the excitation spectrum of the A-type 342 nm emission (dashed curve), but their admixture is already strong at low temperature in contrast to the observation described above without K co-doping.

The main A-type excitation peaks remain at 225 and near 295 nm, but the latter intense peak is now considerably broadened, showing components at ∼290, 297, and ∼312 nm. The existence of A-type centres strongly absorbing in this region explains the disappearance of the weak C-type excitation features above 280 nm for K co-doping. A similar quenching as for $BaBr_2:Ce^{3+}$ is observed for the C-site luminescence, but the C → A switching occurs in the slightly lower temperature range from 80 to 135 K. The quenching of the B-type luminescence is observed at about 100 K. The excitation spectrum of the 410 nm B-type emission (dotted curve in figure 4) also shows important broadening of the main peak near 236 nm, now acquiring a huge shoulder near 222 nm together with enhanced badly resolved high-energy satellites up to ∼337 nm.

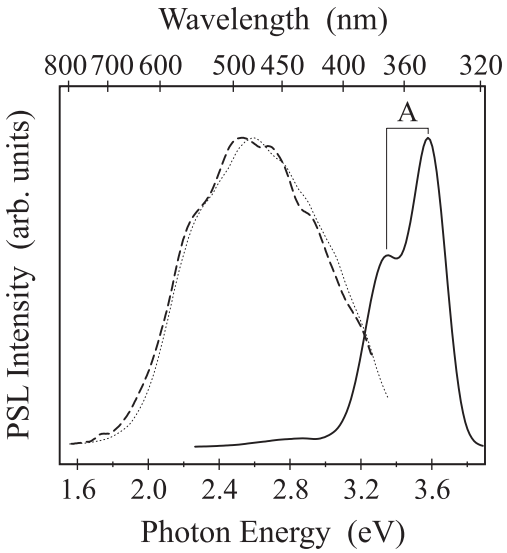

Figure 5. Normalized PSL and PSL stimulation spectra of $BaBr_2$:K:Ce^{3+} after x-irradiation at room temperature. The PSL was stimulated at 500 nm (solid curve); the stimulation was detected at 350 nm (dashed curve). The stimulation spectrum for $BaBr_2$:Ce^{3+} (dotted curve) is shown for comparison (spectrum taken from figure 3, part (a), dashed curve). The spectra were recorded at room temperature.

K co-doping causes practically no changes in the A-type PSL at RT (shown in figure 5). However, there is no B-type emission at RT, whatever the stimulation wavelength, so the overall PSL efficiency is smaller than without potassium doping. Low temperature PSL in K co-doped samples, recorded after x-irradiation at RT, is extremely weak and is due to the cerium B site and partly to the europium impurity (present as an accidental impurity).

Recently low temperature EPR experiments have also been carried out. Preliminary results on the as-grown $BaBr_2$ samples show the presence of multiple Ce^{3+} sites, confirming the luminescence data.

4. Discussion

4.1. Ce^{3+} sites in $BaBr_2$

The main parameters characterizing Ce^{3+} sites A, B, and C in $BaBr_2$ are compiled in table 2 together with data for some comparable compounds mostly reviewed by Dorenbos [16–18]. The C-type luminescence occurs at the highest energies compared to those of A and B and does not appear in PSL (i.e. it is unrelated to charge detrapping processes), while in PL it has the narrowest excitation lines, the smallest d–d splittings [22], and the smallest Stokes shift ΔS. Therefore, the C-type PL may be assigned to isolated Ce^{3+} ions on the unperturbed Ba^{2+} site coordinated by nine Br^- ions in the tricapped trigonal prism (3tp) configuration. Compared with the other bromides in table 2, orthorhombic $BaBr_2$ has by far the largest unrelaxed average ligand distance, explaining the small d–d splittings and the rather moderate redshift D (defined as the depression of the first f $\rightarrow$ d excitation energy with respect to the free Ce^{3+} ion [22]).

At temperatures above 110–150 K, the energy originally exciting the isolated Ce^{3+} ions can apparently be transferred to some kind of nearby perturbed Ce^{3+} site, resulting in the

Table 2. Parameter values for Ce^{3+} luminescence in various matrices: number (N) and average unrelaxed distance (R_{av}) of ligands, wavelength of the first f–d transition in excitation and absorption ($\lambda_{exc/abs}$), the same in emission (λ_{em}), apparent total d–d splitting (ε_{cfs}), redshift (D) of the first absorption transition with respect to the free Ce^{3+} ion, and Stokes shift (ΔS).

Comp./site	N	R_{av} (pm)	$\lambda_{exc/abs}$ (nm)	λ_{em} (nm)	ε_{cfs} (cm^{-1})	D (cm^{-1})	ΔS (cm^{-1})	Reference
$BaBr_2$ (ortho.)								This work
A	9	341	310	342	12 186	17 082	3018	
B	9	341	305	382	$>\sim$10 000	16 960	6610	
C	9	341	302	330	7 851	16 640	2810	
$LaBr_3$	9	312	330	358	8 300	19 037	2370	[16, 18]
$LuBr_3$	6	289[a]	370	405	16 641	22 313	2336	[16, 23]
$BaCl_2$ (cubic)	8	329	334	352	12 610	19 400	1531	[16, 24]
$BaCl_2$ (ortho.)	9	324	325	337	—	18 571	1095	[16, 24]
$LaCl_3$	9	295	281	335	5 565	13 753	5736	[23, 25]
$LuCl_3$	6	274[a]	340	373	18 379	19 928	2602	[16, 18, 23]

[a] Sum of the ionic radii (similar estimates for R_{av} agree within 1% with the crystallographic data listed for the other compounds). Estimates given for $LuBr_3$ and $LuCl_3$ by Dorenbos [17] based on comparisons with other compounds are 274 and 258 pm, respectively.

quenching of the C-type luminescence. Similar quenching is more pronounced for the K co-doped crystal and starts at slightly lower temperatures, which may be understood as a result of a larger number of perturbed Ce^{3+} ions in the vicinity of the fewer isolated Ce^{3+} ions. In both crystals the A-type luminescence is favoured, whose excitation spectrum weakly overlaps the C emission.

Accordingly, the A-type luminescence may be assigned to monovalent background impurities such as K^+, Na^+, etc. Such ions, also substituting for Ba^{2+}, may provide short-range charge compensation for Ce^{3+} ions, which may then yield the A-type luminescence at slightly lower energies. Evidently, the presence of a monovalent compensator adjacent to Ce^{3+} strongly enhances the relaxation of some of the Br^- ligands towards the trivalent rare-earth ion, which is expected to increase the overall d–d splitting and slightly also the redshift as well as the Stokes shift. Several geometries of the Ce^{3+}–K^+ defect are possible, which may become important for larger K concentrations. This may explain the observed broadening and splitting of the A-type excitation bands near 295 and 310 nm seen especially in the K co-doped case. These bands correspond to the lower $5d^1$ levels of Ce^{3+}, which are apparently more strongly perturbed than the highest $5d^1$ level corresponding to the unsplit 225 nm band.

The B site, showing outstanding values in $BaBr_2$ for the Stokes shift, has to correspond to other charge compensators adjacent to the Ce^{3+} ions, causing much stronger perturbation. Candidates are (i) an O^{2-} substituting for a Br^- ion, (ii) defects involving a Ba vacancy (a single Ba vacancy, possibly shared by two ceriums, or a Ba–Br vacancy pair), or (iii) an interstitial Br^- ion. A conclusion in favour of O^{2-} was made in $SrCl_2$, where the first cerium emission line at $\sim$340 nm [24] was shifted by an oxygen containing environment to $\sim$373 nm [26]. In our $BaBr_2$:Ce^{3+} samples the B-type luminescence is invariably present and this may be due to the unavoidable oxygen contamination as suggested by the invariable presence of the 460 nm shoulder in PL and the similarities between the excitation spectra of B type and that seen in $BaBr_2$:O^{2-}. Interstitial anions in halides usually appear only as radiation defects, their production requiring at least excitonic energy, in our case 7–8 eV [20]; however, for our low symmetry lattice and the mismatch (0.11 nm/0.15 nm) of the Ce^{3+}/Ba^{2+} ionic radii this alternative cannot be discarded. In fact compensation by interstitial fluorine ions has been

proposed in CaF_2 [27]. Ba vacancies may also be a viable alternative. Thus, at this stage we prefer the oxygen-associated model for site B, but we have insufficient information to discard the other variants. In any case, the numerous geometries possible for charge compensation explain the large linewidths observed for the B-type spectra. In the vicinity of a monovalent impurity ion these variants may be further modified, which explains further broadening and more redshifted excitation components seen for K co-doping.

The comparison made for some chosen bromide and chloride matrices in table 2 confirms the trends discussed by Dorenbos [16–18] with a possible exception concerning the redshift of the first f–d excitation energy. Instead of increased values of the redshift D in $BaBr_2$ compared to $BaCl_2$, we find appreciably smaller values even for the perturbed sites, in contrast to the other halides where the bromides systematically have larger D values than the respective chlorides, though the differences show strong variations. This cannot be caused only by the large ligand distances in orthorhombic $BaBr_2$, as in $BaCl_2$ these distances are scaled down only by 5%–6% as in other chloride/bromide pairs. The comparison may be influenced by problems in the assignment of the excitation lines for $BaCl_2$ [17, 24] caused by several factors. One of the factors is a possible mixing of the lines due to cubic and orthorhombic phases in the cited experiments [24] aggravated by the small intensities of the respective first f $\rightarrow$ d transitions, the latter property also encountered in our experiments in $BaBr_2$. A second possible cause of the discrepancy may be the effect of impurities on the $BaCl_2$ spectra [24] which compare better with our broadened B-type spectra in figure 4 attributed to the simultaneous perturbations due to unidentified defects and potassium dopants. While the elimination of the first problem could lead to comparable redshifts for both barium salts, accounting for the other might even reverse the situation to comply with the expected trend. Nevertheless, it should be pointed out that the redshifts found by us for all three sites in undoped orthorhombic $BaBr_2$ are the smallest reported to our knowledge for Ce^{3+} in bromides.

4.2. Charge trapping and transfer processes

X-irradiation mostly generates free electron polarons and holes hopping like Br_2^{2-}-type small polarons. For the stabilization of these charges at RT lattice defects of an appropriate kind are required. In lattices where cerium substitutes for trivalent cations, holes mostly become trapped at Ce^{3+} ions forming Ce^{4+} (see e.g. Cs_2NaYF_6:Ce [28]). For divalent substitution sites this is less likely, but holes may still be aggregated with cerium complexes. It should be taken into account that the dipolar moments of charge-compensated defects such as our cerium complexes A and B are able to attract either charge, depending on the relative orientation of the dipole moment with respect to the location of the free charge. As shown by experiment, the PSLs of types A and B correspond to distinct processes each consisting of a specific ionization event followed by recombination and a specific cerium luminescence. As we will see, this also indicates that the defects involved in a given elementary PSL process are spatially correlated.

As indicated by the PSL stimulation spectra, anion vacancies have to be considered as electron traps in the first place. In fact the broad absorption bands near 485 and 550 nm observed as PSL stimulation bands of types A and B, respectively, apparently correspond to F-type centres. Compared to the absorption of the unperturbed F centres [8] its absorption is only slightly broadened (by a few per cent); the A-type F centre shows a centroid blueshift of $\sim$0.3 eV, while the B-type F centre is practically unshifted. However, for the A-type F centre the shift goes in the opposite direction compared to the one observed for the $F_A(K^+)$ centre in $BaBr_2$:K (where the presence of a K^+ ion on a Ba^{2+} site next to the anion vacancy causes a redshift of the absorption by $\sim$0.14 eV, without an increase of the overall component splitting [10]). This can be understood as the effect of a perturbing cation with a positive

surplus charge in our case, i.e. the F centre feels the presence of a Ce^{3+} (or Ce^{4+}) ion, meaning that the A-type F centre in question is apparently situated closer to the more positive end of a Ce^{3+}–K^+ dipole. The B-type F centres on the other hand seem to be very weakly perturbed, if at all, the PSL stimulation spectra monitoring nearly isolated F centres still preferentially located in the proximity of compensated Ce^{3+} ions of B type.

As the holes can be assumed to remain trapped during PSL stimulation, playing the role of recombination centres, the fingerprint character of the emission indicates that they are close to the specific cerium complexes. Holes trapped at other sites (e.g. at isolated O^{2-} or K^+ centres) may also recombine, but the liberated energy will not be transferred into specific emission if the cerium complex is far away. Therefore, holes involved in A-type PSL should preferentially be trapped near dipolar Ce^{3+}–K^+ defects, while the holes active in B-type PSL must be trapped near Ce^{3+} defects compensated by some other unidentified defect (an O^{2-} substituting for a Br^- ion, a Ba vacancy defect, or an interstitial Br^- ion). Radiation-induced interstitial halogen atoms or diamagnetic halogen aggregates near the respective cerium complexes are less probable as this would require the generation of anionic Frenkel pairs not found up to now in undoped $BaBr_2$ [10] and in $BaBr_2:Eu^{2+}$ [9]. In these cases no O^- defects have been found either.

The fingerprint character of the PSL features is clearest in the room temperature spectra of $BaBr_2:Ce^{3+}$, where B- *and* A-type PSL take place at the same time. Both the trapped electron and the trapped hole involved in a recombination event are located fairly close to the same cerium complex emitting their recombination energy. Even if recombination does not necessarily reunite the same electron–hole pair generated in an x-ray ionization event, most partners may be assumed to remain close to the ionization site and become trapped in the vicinity of the nearest Ce complexes. A similar situation was described for $BaFBr:Eu^{2+}$, with the distances of the trapped components estimated from spin–lattice relaxation effects as a few lattice constants [29], while the average distance between rare-earth activators for a concentration of 1000 ppm is only slightly larger. Such order of magnitude estimates, providing an excellent spatial resolution for the x-ray imaging application in the absence of light scattering, seem to be appropriate in our case as well, given the large characteristic shift of the A-type F centres, and the requirement of efficient energy transfer from the hole sites to the cerium.

We still have to discuss questions about the disappearance or absence of PSL types. The low temperature quenching of the A-type luminescence in $BaBr_2:Ce^{3+}$ may be caused by a specific thermally activated step in this PSL, which may be either the thermal ionization of the excited A-type F centre, or the transfer of the recombination energy from the hole site to the cerium A site. This effect seems to be absent for B-type PSL, indicating perhaps a specific difference caused by the presence of the different charge compensators. The absence of C-type PSL at all temperatures suggests that the radiation-induced holes are never trapped close to isolated Ce^{3+} ions (which is quite natural for a positively charged crystal defect), and tend to migrate towards compensated Ce sites. This observation again supports the assignment of the C site. Similarly, the thermally stimulated energy transfer observed in PL from the C to the A site may also be related to the uncompensated charge of the isolated Ce^{3+}.

5. Conclusion

We have shown that two kinds of the observed room temperature luminescence in orthorhombic $BaBr_2:Ce^{3+}$ can be explained in a natural way, ascribing them to charge-compensated Ce^{3+} centres, one type associated with potassium (or some other monovalent cation) on a Ba^{2+} site and another one with an unidentified defect. These complexes are active both in photoluminescence and luminescence stimulated at lower energies following x-ray irradiation.

A third type of photoluminescence observed only at low temperatures is ascribed to more or less isolated cerium ions. The PL of the isolated Ce^{3+} has outstanding parameters due to the high number (nine) of similar Br^- ligands and their large average distance from the rare-earth ion. Even for the perturbed sites the redshift of the first f–d excitation energy of the luminescence is smaller than reported for $BaCl_2$, contradictory to findings in other pairs of bromide/chloride matrices. This indicates that a re-examination of the phase distributions and assignments in the case of $BaCl_2$ might be necessary.

The PSL spectra, observed following x-ray ionization, are almost comparable in intensity to the case of the BaFBr:Eu^{2+} single crystal. The existence of two distinct PSL types indicates that the recombining electron–hole pairs are only weakly separated, the members of a pair being trapped in the vicinity of the same cerium–impurity complex. The electrons are trapped in F-type centres whose band position is characteristic for the nearby charge-compensated Ce complex whose fingerprint is also seen on the PSL.

Acknowledgments

The authors would like to thank the Deutsche Forschungsgemeinschaft for financial support. Funding by the Hungarian Scientific Research Fund (OTKA T 034262), the Center of Excellence Program (contract No ICA1-2000-70029 EU), and the NATO Scientific Fellowship Programme (2022/NATO/02) is also gratefully acknowledged.

References

[1] Schweizer S 2001 *Phys. Status Solidi* a **187** 335
[2] Edgar A, Spaeth J-M, Schweizer S, Assmann S, Newman P J and MacFarlane D R 1999 *Appl. Phys. Lett.* **75** 2386
[3] Schweizer S, Corradi G, Edgar A and Spaeth J-M 2001 *J. Phys.: Condens. Matter* **13** 2331
[4] Edgar A, Secu M, Williams G V M, Schweizer S and Spaeth J-M 2001 *J. Phys.: Condens. Matter* **13** 6259
[5] Secu M, Schweizer S, Spaeth J-M, Edgar A, Williams G V M and Rieser U 2003 *J. Phys.: Condens. Matter* **15** 1097
[6] Brackett E B, Brackett T E and Sass R L 1963 *J. Phys. Chem.* **67** 2132
[7] Grujic D, Houlier B, Yuste M, Taurel L and Chapelle J P 1970 *C. R. Acad. Sci. (France)* **270** 1355
[8] Houlier B 1977 *J. Phys. C: Solid State Phys.* **10** 1419
[9] Secu M, Schweizer S, Rogulis U and Spaeth J-M 2003 *J. Phys.: Condens. Matter* **15** 2061
[10] Moreno M 1977 *Cryst. Lattice Defects* **7** 27
[11] Moreno M 1975 *Solid State Commun.* **16** 1239
[12] Rogulis U 2003 private communication
[13] Song K S and Williams R T 1993 *Self-Trapped Excitons* (*Springer Series in Solid State Sciences* vol 105) (Berlin: Springer)
[14] Iwase N, Tadaki S, Hidaka S and Koshino N 1994 *J. Lumin.* **60/61** 618
[15] Secu M, Kalchgruber R, Schweizer S, Spaeth J-M and Edgar A 2002 *Radiat. Eff. Defects Solids* **157** 957
[16] Dorenbos P 2000 *J. Lumin.* **91** 155
[17] Dorenbos P 2000 *Phys. Rev.* B **62** 15650
[18] Dorenbos P 2001 *Phys. Rev.* B **64** 125117
[19] Monberg E and Ebisuzaki Y 1974 *J. Cryst. Growth* **21** 307
[20] Nicklaus E 1979 *Phys. Status Solidi* a **53** 217
[21] Rogulis U, Schweizer S, Secu M and Spaeth J-M 2004 *J. Phys.: Condens. Matter* in preparation
[22] Dorenbos P 2000 *Phys. Rev.* B **62** 15640
[23] Guillot-Noël O, de Haas J T M, Dorenbos P, van Eijk C W E, Krämer K and Güdel H U 1999 *J. Lumin.* **85** 21
[24] Li W-M and Leskelä M 1996 *Mater. Lett.* **28** 491
[25] Andriessen J, Antonyak O T, Dorenbos P, Rodnyi P A, Stryganyuk G B, van Eijk C W E and Voloshinovskii A S 2000 *Opt. Commun.* **178** 355
[26] Antonyak O T and Pidzyrailo N S 1986 *Opt. Spectrosc.* **60** 743
[27] Manthey W J 1973 *Phys. Rev.* B **8** 4086
[28] Pawlik Th and Spaeth J-M 1997 *J. Appl. Phys.* **82** 4236
[29] Koschnick F K, Spaeth J-M and Eachus R S 1992 *J. Phys.: Condens. Matter* **4** 8919